Model Independent Approach to the Single Photoelectron Calibration of Photomultiplier Tubes

R. Saldanha[a,b,c,1,*], L. Grandi[a,b,c], Y. Guardincerri[d,a,2], T. Wester[a,c]

[a]Kavli Institute for Cosmological Physics, University of Chicago, Chicago, IL 60637, USA
[b]Enrico Fermi Institute, University of Chicago, Chicago, IL 60637, USA
[c]Department of Physics, University of Chicago, Chicago, IL 60637, USA
[d]Fermi National Accelerator Laboratory, Batavia, IL 60510, USA

Abstract

The accurate calibration of photomultiplier tubes is critical in a wide variety of applications for which it is necessary to know the absolute number of detected photons or precisely determine the resolution of the signal. Conventional calibration methods rely on fitting the photomultiplier response to a low intensity light source with analytical approximations to the single photoelectron distribution. We show that this approach often leads to biased estimates due to an inability to model the full distribution accurately, especially at low charge values. We present a simple statistical method to extract the relevant single photoelectron calibration parameters (first two central moments) without making any assumptions about the underlying single photoelectron distribution. We illustrate the use of this method through the calibration of a Hamamatsu R11410 photomultiplier tube and study the accuracy and precision of the method using Monte Carlo simulations. The method is found to have significantly reduced bias compared to conventional methods and works under a wide range of light intensities, making it suitable for the simultaneous calibration of large arrays of photomultiplier tubes where uniform illumination may not be possible.

Dedication: This paper is dedicated to the memory of Yann Guardincerri, a wonderful colleague and a dear friend.

Keywords: photomultiplier tubes, single photoelectron response, calibration

1. Introduction

Photomultiplier tubes (PMTs) are widely used to detect low levels of light in scientific experiments, medical instruments, and industrial equipment. PMT operation is typically divided into two regimes - photon counting, where the rate of detected photons is small compared to the timing resolution of the detector such that individual photoelectron pulses do not overlap, and signal integration, for light sources of higher intensities where individual photoelectron signals cannot be distinguished. In the latter case, for applications in which the resolution of the signal plays an important role, such as scintillation spectroscopy or pulse shape discrimination, it is critical to obtain an accurate estimate of the total number of generated photoelectrons, as well as the relative standard deviation of the single photoelectron distribution, since these are often the dominant contributors to the resolution of the signal. The response of a PMT is therefore typically calibrated relative to the mean of the charge distribution corresponding to a single photoelectron (SPE). Knowledge of the PMT SPE response is also necessary in order to combine the output signals from several different PMTs operating at different gains.

In this work we present a simple statistical

---

method to determine the essential parameters of the SPE response of a photomultiplier tube without making any assumptions about the shape of the SPE spectrum. Unlike conventional methods which typically rely on fitting the output charge distribution with a model describing the SPE spectrum, we use the known statistical properties of the PMT response to obtain the calibration parameters directly from the charge distribution, without requiring a fit. The general statistical nature of the method allows it to be applied to any kind of photomultiplier tube and to a wide range of illumination levels while only requiring a pulsed light source, a device that is already commonly implemented in scintillation detectors.

2. Conventional Methods

The standard method to calibrate the SPE response of a PMT is to use a low intensity light source such that the probability of generating more than a single photoelectron within the time resolution of the detector is small. The resulting spectrum of the integrated signal is then fit with a parameterized model of the SPE response, in order to obtain the mean and variance for each individual PMT. The difficulty of such a method lies in the choice of the model. Electron multiplication within the dynode chain is a branching process where the output charge at the PMT anode depends on the secondary electron emission probability at each dynode. For the typical photoelectron, i.e. one generated at the photocathode, the most commonly used approximation is a standard Gaussian distribution [1], where the mean of the single photoelectron distribution is simply taken as the peak, though more complicated models [2, 3] are also used to try and accurately model the electron cascade process. Additionally, a large variety of sub-optimal trajectories of photons and electrons through the PMT are also possible. For example, a photon may pass through the cathode and directly strike the first dynode [4, 5], a photoelectron may inelastically backscatter off the first dynode [6, 5] or skip a dynode stage [7]. Such trajectories often lead to under-amplified photoelectron signals, increasing the component of the SPE spectrum with less charge than that at the peak. Since these under-amplified photoelectrons are generated during normal operation and contribute to the total integrated signal, they should

be included when estimating the mean and variance of the SPE response. Under-amplified photoelectrons can account for as much as 20% of the SPE spectrum in some models of PMTs, decreasing the mean of the SPE response by 10-20% relative to the peak [8, 9]. Ignoring the contribution of under-amplified photoelectrons can lead to an underestimate of the number of detected photoelectrons and an incorrect estimate of the resolution.

The true shape of the under-amplified component is often difficult to determine due to the large overlap with contributions from electronics noise. Several authors have proposed adding additional terms to the fit function of the single photoelectron response, including a falling exponential, and additional Gaussian components [9, 10]. However, the relative weight and shape of the under-amplified component can vary with the type of photocathode and dynode structure, and can even differ for individual PMTs of the same model and gain [4, 8]. Thus it is often difficult to construct a parameterization of the single photoelectron spectrum that is suitable for a range of PMTs and conditions.

3. Model-Independent Method

The single photoelectron calibration method presented here focusses on accurately estimating the mean and variance of the SPE distribution at the PMT output, including contributions from underamplified photoelectrons, without making any assumptions about the shape of the distribution. For most experimental purposes, knowledge of the higher moments, or the entire functional form of the SPE response is not required. We assume that the PMT will be used within its linear regime and this ensures that, as the number of photoelectrons increases, the response to multiple photoelectrons quickly converges (by the central limit theorem (CLT)) to a Gaussian distribution that is completely described by the first two central moments of the single photoelectron response. This is illustrated in Figure 1, which shows the charge spectra from 1, 2, 5, and 10 photoelectrons where each photoelectron is randomly and independently drawn from an SPE distribution with a large fraction of under-amplified photoelectrons. Even in this case the response to $n \geq 5$ photoelectrons (PE) is to a very good approximation Gaussian, with a mean and variance n times that of the entire SPE distribution. Though
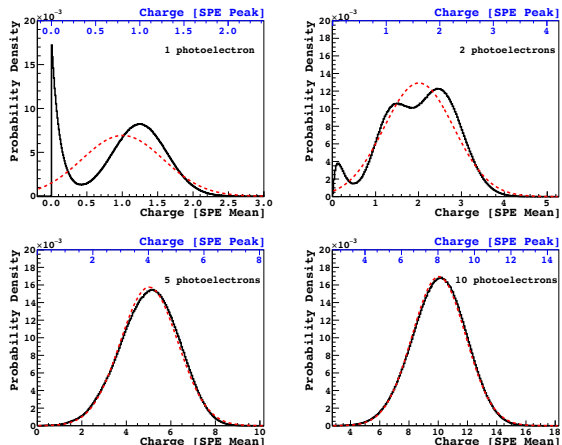
Figure 1: Solid Line: Simulated charge distribution of 1, 2, 5 and 10 photoelectrons for a PMT with a Gaussian distribution of fully-amplified photoelectrons and a large exponential component of under-amplified photoelectrons. Background noise was not included in the simulation. Dashed Line: Gaussian distribution with the same total mean and variance as the corresponding PMT charge distribution. The bottom axis shows the charge calibrated with respect to the true SPE mean, while the top axis is calibrated with respect to the peak of the fully-amplified photoelectrons.

the distribution converges to a Gaussian for large number of photoelectrons, it is critical to include the under-amplified component in the estimate of the mean and variance in order to obtain the correct estimate of the photoelectron statistics in the signal. For example, if one were to calibrate the SPE mean as simply the Gaussian peak position of the SPE distribution in the top left panel of Figure 1, one would obtain an SPE mean a factor 1.25 higher than the true mean. Using this incorrect value would result in a 20% [(1.25-1)/1.25] underestimate of the true number of photoelectrons in the other panels (or any given signal). We note that the above considerations also apply when the light is distributed over an array of photomultipliers, and the total signal is obtained by summing the output of all the PMTs. In this case, even though the SPE responses of the individual PMTs are not necessarily identical, variants of the classical CLT typically ensure convergence to a Gaussian distribution. Thus, for scintillation signals that produce more than 5 PE on average, the contribution of the photomultiplier response is determined by only the first two central moments of the SPE distribution.[3]

In order for the description of the method to be clear, we must first briefly describe the corresponding experimental setup. A low intensity, pulsed laser is used to illuminate the PMT to be calibrated. The laser is externally triggered and for each trigger the PMT output is integrated at the time corresponding to the expected anode output signal. We stress that in this setup the PMT's output for every trigger is recorded, even if there is no visible signal. This ensures that no under-amplified photoelectrons are missed.

For every trigger, there are two contributions to the total measured charge q, one from the background noise that is always present in the system, regardless of the presence or absence of a laser-induced photoelectron signal, and one associated with the presence of a photoelectron signal. The total integrated charge is simply the sum of these two contributions, which, by definition, are independent. We will denote the probability distribution of the total integrated charge as $T(q)$, and the background and signal probability distributions as $B(q)$ and $S(q)$ respectively. It then follows that

$$T(q) = (B * S)(q) \tag{1}$$

where $*$ indicates a convolution of the two distributions. For independent random variables, the first two moments are additive, and hence

$$\boldsymbol{E}[T] = \boldsymbol{E}[B] + \boldsymbol{E}[S] \tag{2}$$
$$\boldsymbol{V}[T] = \boldsymbol{V}[B] + \boldsymbol{V}[S] \tag{3}$$

where $\boldsymbol{E}[X]$ and $\boldsymbol{V}[X]$ denote the mean and variance of the distribution X respectively, and we have omitted the domain of the distributions for clarity.

The signal charge distribution can be written in terms of the number of photoelectrons p produced

$$S(q) = \sum_{p=0}^{\infty} S_p(q) L(p) \tag{4}$$

where $S_p(q)$ is the signal charge distribution corresponding to exactly p photoelectrons and $L(p)$ is the discrete probability distribution of the number of photoelectrons produced in a single laser pulse. We shall denote the charge distribution of the

_____

[3]For smaller signals, the knowledge of the mean and variance are still necessary for calibration, and are still accu-

rately estimated by the method described in this paper, though higher moments may also need to be calculated to fully model the shape of the detector response.

SPE response as $S_1(q) \equiv \psi(q)$. Assuming that the PMT response is linear, the multi-photoelectron response $S_p(q)$ is the p-times repeated convolution of $\psi(q)$, denoted as $S_p(q) \equiv \psi^p(q)$. The mean and variance of these two distributions are related by $E[\psi^p] = p \cdot E[\psi]$ and $V[\psi^p] = p \cdot V[\psi]$. Using these two properties one can calculate the mean and variance of the signal

$$E[S] = E[\psi] \cdot E[L] \qquad (5)$$

$$V[S] = V[\psi] \cdot E[L] + E^2[\psi] \cdot V[L] \qquad (6)$$

Finally, we can substitute the above in Eqs. (2) and (3) to obtain the first two central moments of the single photoelectron response $\psi(q)$

$$E[\psi] = \frac{E[T] - E[B]}{E[L]} \qquad (7)$$

$$V[\psi] = \frac{V[T] - V[B] - E^2[\psi] \cdot V[L]}{E[L]} \qquad (8)$$

As can be seen from the above equations, in order to obtain the mean and variance of the SPE distribution, one needs to know the mean and variance of the photoelectron distribution $L(p)$.

For an ideal laser emitting coherent light in a single mode, the distribution of the number of photons follows a Poisson distribution [11], with the variance equal to the mean. Even in the case where the emitted light is not perfectly Poissonian, it can be shown that after a random deletion process (such as attenuation by optical filters or conversion to photoelectrons with non-unity quantum efficiency) the output distribution approaches a Poisson distribution with reduced mean [12, 13]. Explicitly, if the initial photon distribution has a ratio of the variance to the mean (defined as the Fano factor), F_i, then after attenuation by a factor η, the Fano factor F_o of the output distribution is

$$F_o = 1 + \frac{(F_i - 1)}{\eta}$$

Thus even for non-ideal light sources, if the output is strongly attenuated ($\eta \gg 1$), $F_o \approx 1$ and the variance approaches the mean, as for a Poisson distribution. Given these considerations, we can assume that the distribution of detected photons from a strongly attenuated laser light source follows a Poisson distribution. We can therefore further simplify Eq. (8) by setting the variance of

the photoelectron distribution equal to the mean, $V[L] = E[L]$, to get:

$$V[\psi] = \frac{V[T] - V[B]}{E[L]} - E^2[\psi] \qquad (9)$$

Before discussing the method to estimate the parameters on the right hand side of Eqs. (7) and (9) it is worthwhile to explicitly list some of the assumptions made above and compare them to other methods of single photoelectron calibration.

- Unlike fitting methods, we have not assumed any functional form for the SPE response. The above equations are valid for any SPE distribution with no assumptions about the shape or amplitude of the under-amplified photoelectron distribution.

- Similarly, we have also made no assumption about the shape of the background noise distribution, which is determined by the specific electronics used and the background noise present in the setup.

- As with most fitting methods, we have assumed that the PMT and any associated electronics respond linearly to the number of photoelectrons. In the typical regime used by this method, fewer than 20 PE are produced in each laser pulse, which is well within the linear range of most PMTs.

- The above formulation divides the contributions of the total charge into two categories, background and signal. The background distribution accounts for all signals that are independent of the photoelectron production by the laser. This includes any noise from the electronics, the trigger and the pulsing of the laser (which occurs for every trigger) as well as dark count signals produced by thermionic emission from the photocathode and dynode chain. The signal distribution is assumed to only include contributions that are linear with the number of laser-induced photoelectrons. In certain experimental setups, there may be contributions that do not fall into either category. For example, noise from a discriminator firing (when the signal is above a certain threshold) may only occur when the laser light produces a signal, but it does not increase as the number of photoelectrons increases. In such cases, as with other calibration methods, care must be taken to account
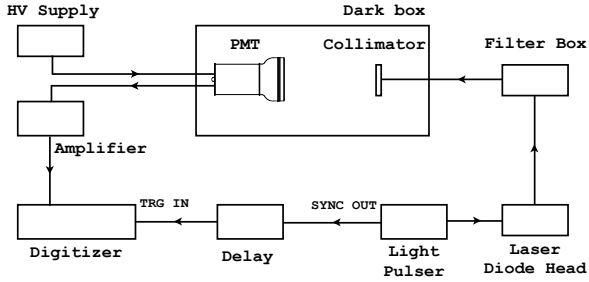
4

Figure 2: Schematic diagram of the experimental setup used to measure the single photoelectron spectrum with a pulsed laser light source.
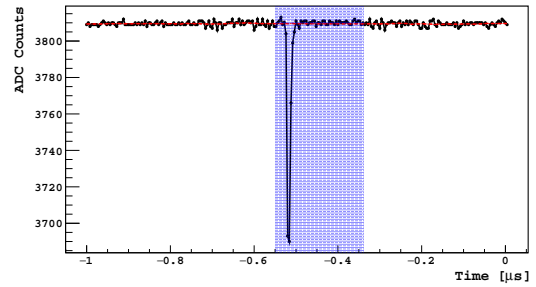

Figure 3: Example of a digitized PMT signal within a sample trigger window, acquired during a laser data set. The black points indicate the digitized waveform, with the dashed horizontal line showing the estimated baseline. The shaded region indicates the fixed laser time window chosen for integration. The negative pulse in the laser time window likely indicates the presence of a laser-induced photoelectron signal.

for these contributions in the total charge distribution.

- The shape and relative contribution of under-amplified photoelectrons to the SPE spectrum can depend on various factors such as external magnetic fields, non-uniformity of the photocathode, the intensity and angular distribution of light incident on the photocathode, etc. As with all calibration methods, it is therefore important that the setup and illumination of the PMT during calibration be as close as possible to that of the PMT during its regular operation.

4. Experimental Setup

In order to test the calibration method described above we have used the experimental setup illustrated in Figure 2. A Hamamatsu R11410 3" photomultiplier with a 12 stage box and linear-focused dynode structure [14] was placed in a custom-made metal darkbox that featured a continuous conducting surface to reduce the effect of electrical noise. The cathode was maintained at negative high voltage with a total divider resistance of 37 MΩ between the cathode and the anode, and the recommended voltage distribution ratio[4] between the dynode stages. The PMT was illuminated by a collimated optical fibre that carried light from a fast pulsed laser diode (Hamamatsu PLP-10-040C [14]) which we will henceforth refer to as a laser. The laser pulses had a typical width of 60 ps (FWHM) and a wavelength of 405 nm. The intensity of the light incident on the PMT was varied by placing different neutral

density filters along the light path. For all data sets acquired, the combined attenuation factor η of the filters was kept $\geq 10^5$, in order to ensure that the photon distribution was Poissonian. The anode of the PMT was terminated with a 50 Ω resistor and connected to a custom fast amplifier with a 10x gain. The output of the amplifier was then sent to a 12 bit, 250 MHz CAEN V1720 digitizer [15]. The digitizer was externally triggered by the synchronous output of the laser, delayed by 500 ns with respect to the optical signal; this avoids any noise related to the triggering of the digitizer from overlapping with the PMT output in the time window of interest. For each trigger a 1 μs digitized waveform was recorded and stored for analysis offline.

For each configuration of light intensity and PMT voltage that was studied, two data sets of $N = 500,000$ triggers were acquired at a trigger rate of 1 kHz. A "laser" data set was acquired with the optical fibre connected such that the laser light illuminated the PMT and another "blank" data set was acquired with the optical fibre disconnected before the filter box, and the fibre feedthrough capped. As will be described in detail in the next section, the laser data set will be used to estimate the moments of the total charge distribution (signal + background), the blank data set will be used to estimate the moments of the background charge distribution, and the combination of both will be used to estimate the photoelectron distribution. In order to ensure that the noise levels remained the same for both the laser and blank data, all the electronics (including the laser)

---

[4]4:1.5:2:1:1:1:1:1:1:1:1:2:1

5

and wiring were kept in the same operating conditions for both runs. As a consistency check, for a few configurations, a blank data set was taken before and after the laser data set and the integrated charge distribution for the two blank data sets were compared using the Kolmogorov-Smirnov test. In all cases, the integrated charge spectrum of the blank data sets were found to be compatible (p-value > 0.1).

The event reconstruction required for this calibration method is straightforward. The expected time window for the laser-induced PMT signal is identified empirically by averaging together all the waveforms acquired during a laser data set and then selecting a 208 ns time window to include the entire laser-induced signal. Note that the chosen window should start early enough to include signals from photons passing through the photocathode and directly striking the first dynode [5]. Outside of the laser time window a baseline is calculated for each individual waveform using a moving average of $\pm$ 20 ns around each sample. The baseline within the laser time window is then linearly interpolated using the samples on either side of the window. This method ensures that the baseline is evaluated in the same way regardless of whether or not a laser signal is present. A sample waveform along with the defined laser time window and estimated baseline is shown in Figure 3.

The integral (inverted to account for the negative PMT pulses) of the baseline-subtracted waveform over the defined laser time window is calculated for each trigger. Figure 4 shows the distribution of the integral for a laser and a blank data set, acquired at an absolute PMT voltage difference of 1700 V ($\approx 1.6 \times 10^7$ gain) and a filter attenuation of 5×10^{-6}. In both distributions the peak centered at zero is primarily due to fluctuations of the noise about the estimated baseline with no photoelectron signal present. The peak at 400 count·samples in the laser data is due to fully amplified single photoelectrons from the photocathode, and a peak due to two fully amplified photoelectrons at 800 count·samples is also visible. The small peak at 400 count·samples in the blank data is due to dark noise photoelectrons and possibly small amounts of stray light entering the darkbox ($< 0.2\%$ of triggers) that accidently fall within the laser time window. Since the spectrum of dark-noise photoelectrons does not necessarily follow the same distribution as photon-induced
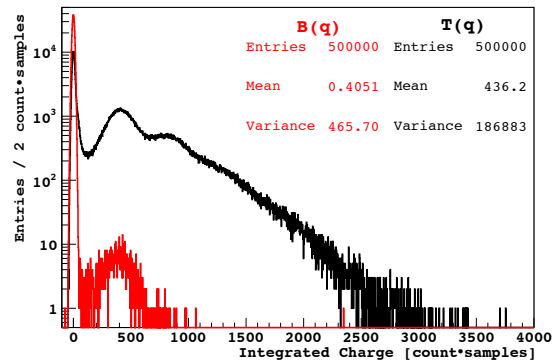

Figure 4: Integrated charge spectra acquired at an absolute PMT voltage difference of 1700 V. The laser data spectrum, $T(q)$, had an estimated occupancy of 1.37 photoelectrons/trigger, while the blank data spectrum, $B(q)$, was acquired at the same settings as the laser data set, but with the optical fibre disconnected.

photoelectrons [9, 6], the presence of these events in both the blank and laser data allows us to correctly account for them and exclude them from the estimation of the single photoelectron mean.

5. Parameter Estimation

As can be seen from Eqs. (7) and (9), in order to determine the first two central moments of the SPE response we need to evaluate the first two central moments of the total charge distribution and the background distribution, as well as the mean number of photoelectrons produced in each trigger. Since we do not have prior knowledge of the true underlying distributions, we will estimate the moments from the experimentally measured data sample of N triggers.

The central moments of the total charge distribution can be directly obtained by calculating the mean and variance of the measured PMT output spectrum in the presence of the laser, which is typically the spectrum that is used to fit the SPE response in other methods. An example spectrum is shown in Figure 4, along with the calculated mean $E[T]$, and variance $V[T]$, to be used in Eqs. (7) and (9).

There is often an overlap of the background distribution and the signal distribution of under-amplified single photoelectrons. This makes it difficult to cleanly determine the mean and variance of the background in the presence of the laser signal. For this reason we estimate the moments of the background spectrum from the separately

measured blank data set, an example of which is shown in Figure 4, along with the calculated mean $E[B]$, and variance $V[B]$.

The only parameter that is not straightforward to estimate is the mean number of laser-induced photoelectrons produced in each trigger, $E[L]$, which we shall refer to as occupancy. As discussed previously, the number of photoelectrons produced follows a Poisson distribution, which can be written as

$$L(p) = \frac{\lambda^p e^{-\lambda}}{p!} \tag{10}$$

$$\lambda \equiv E[L] = V[L] \tag{11}$$

The occupancy λ is directly related to the probability of producing zero laser-induced photoelectrons,

$$\lambda = -\ln(L(0)) \tag{12}$$

which can be estimated from the number of sample triggers with zero laser-induced photoelectrons (zero-pe triggers), N_0, and the total number of sample triggers N

$$\widehat{\lambda} \equiv -\ln(\widehat{N_0}/N) \tag{13}$$

where $\widehat{\lambda}$ and $\widehat{N_0}$ denote the estimates of the occupancy and number of zero-pe triggers in the laser data sample respectively.

There are several different techniques that can be used to estimate the value N_0 and the optimal method will depend on the nature of the signal and background distributions. For example, if the temporal shape of the PMT output pulse is known, and the triggers are individually recorded, one can assign a likelihood for the presence of a laser-induced signal to each individual trigger. For the purposes of this paper, we will restrict ourselves to a very simple algorithm, whose statistical and systematic uncertainties can be estimated analytically.

We will use the fact that we have access to a pure sample of zero-pe events from the blank data set and hence have empirical information about the shape of the zero-pe distribution.[5] Triggers in the laser data set that contain a non-zero number of laser-induced photoelectrons typically have

a higher charge output than triggers that only contain background noise. We can therefore use the comparison of the number of events in low-charge region of the laser and blank spectrum to estimate the number of zero-pe triggers as follows:

1. We place a threshold cut at a low charge value such that the fraction of laser triggers with a non-zero number of laser-induced photoelectrons that fall below the cut is expected to be small (we will quantify this requirement in Section 6.2). We count the number of triggers, A_T, in the laser data set below the threshold and assume they are only zero-pe triggers.

2. In order to get the total number of zero-pe triggers in the laser sample, N_0, we use the shape of the blank spectrum to correct the value of A_T for the number of zero-pe triggers that fall above the threshold. We define the fraction of blank data samples that fall below the threshold cut as f. The estimated total number of zero-pe triggers in the laser data set is then

$$\widehat{N_0} = \frac{A_T}{f} \tag{14}$$

Our estimate for $\widehat{\lambda}$ is therefore

$$\widehat{\lambda} = -\ln(A_T/fN) \tag{15}$$

Rather than expressing the position of the threshold cut in terms of a charge value, which will depend on the shape of the background distribution, we will express it in terms of f, the fraction of the background distribution that falls below the threshold. This not only lets us describe the choice of threshold in a way that can be easily translated to different experimental setups, but, as we will see in the next sections, the statistical and systematic uncertainties are also conveniently expressed in terms of the fraction, f.

6. Parameter Uncertainties

In order to find the optimal operating parameters for the laser intensity and number of triggers, it is useful to calculate the statistical and systematic uncertainties corresponding to the estimate of the moments from the finite data sample.

---

[5]Note that while some blank data events may contain photoelectron signals due to stray ambient light or dark noise, by construction all events have zero laser-induced photoelectrons.
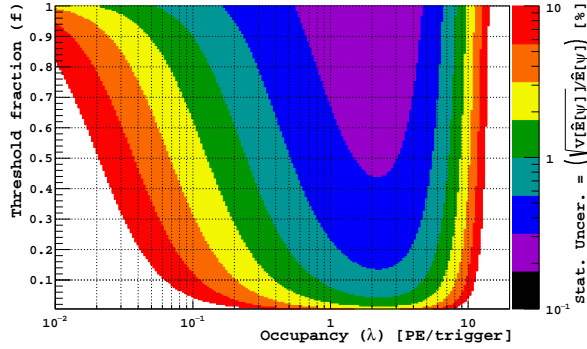
Figure 5: Statistical uncertainty of the model independent method as a function of the occupancy and the fraction of the background spectrum below the threshold cut. Values are calculated using Eq. (16) with the parameters of our experimental setup.

6.1. Statistical Uncertainties

We can calculate the statistical fluctuations in the estimate of the single photoelectron mean as (see Appendix A for derivation)

$$
V\left[\widehat{E}\left[\psi\right]\right] \approx \frac{\lambda(E^2\left[\psi\right] + V\left[\psi\right]) + 2V\left[B\right]}{N\lambda^2}
+ \frac{E^2\left[\psi\right]\left(e^\lambda + 1 - 2f\right)}{fN\lambda^2} \quad (16)
$$

where $\widehat{E}\left[\psi\right]$ denotes the estimated SPE mean, *i.e.* the estimate of the mean of the SPE distribution from the finite data sample acquired. The statistical uncertainty of the estimated single photoelectron mean decreases as the number of trigger samples N increases, with the optimal value for the occupancy depending on the given photomultiplier and the background spectrum. Figure 5 shows how the statistical uncertainty of the SPE mean estimate, evaluated with Eq. (16), varies as a function of the occupancy and f for the parameters of our experimental setup. The statistical uncertainty has a broad minimum at an occupancy value of $\lambda \approx 2$ and decreases as f, the fraction of background events falling below the chosen threshold, increases. The second term in Eq. (16), associated with the statistical uncertainty in the estimation of the occupancy, dominates the overall statistical uncertainty; hence, the precision of this method is strongly dependent on the precision with which the occupancy can be determined.

The statistical uncertainty in the estimated single photoelectron variance is difficult to express analytically and was therefore evaluated using the simulations described in Section 8. It is largely dominated by the statistical uncertainty in the estimation of the occupancy and can be approximated as

$$
V\left[\widehat{V}\left[\psi\right]\right] \approx \left(\frac{\partial \widehat{V}\left[\psi\right]}{\partial \widehat{E}\left[L\right]}\right)^2 V\left[\widehat{E}\left[L\right]\right] + \dots
$$
$$
= \frac{\left(E^2\left[\psi\right] - V\left[\psi\right]\right)^2 \left(e^\lambda + 1 - 2f\right)}{fN\lambda^2} \quad (17)
$$

where we have only considered the dominant term in the first-order Taylor expansion.

6.2. Systematic Uncertainties

The dominant systematic uncertainty in the estimate of the SPE mean arises from the evaluation of the occupancy. The calculation of the occupancy is made under the assumption that the number of non-zero-pe triggers falling below the threshold cut is negligible. However measurements of signals from photomultiplier tubes operated at high gain have shown contributions from under-amplified photoelectrons of arbitrarily small charge [4, 8]. Triggers with a laser-induced photoelectron that produces a very small integrated charge can fall below the threshold cut and be incorrectly included in the calculated number of zero-pe triggers A_T. This leads to a systematic decrease in the estimated occupancy $\widehat{\lambda}$, and correspondingly a systematic increase in the estimated SPE mean.

The estimated SPE mean, $\widehat{E}\left[\psi\right]$, averaged over a large number of measurements, $E\left[\widehat{E}\left[\psi\right]\right]$, can be expressed in terms of the true SPE mean, $E\left[\psi\right]$, as (see Appendix B)

$$
E\left[\widehat{E}\left[\psi\right]\right] \approx E\left[\psi\right] \cdot \left(1 + \frac{k(f)}{f}\right) \quad (18)
$$

where $k(f)/f$ is the ratio of $k(f)$, the fraction of single photoelectron triggers falling below the threshold cut, to f, the fraction of the blank background spectrum below the cut. The value of $k(f)$ depends not only on the the location of the threshold cut, but also on the shape of the SPE spectrum and the operating gain of the PMT. $k(f)$ decreases as the gain increases and typically decreases faster than f as the position of the threshold cut is lowered. Therefore, in order to minimize the systematic bias in the estimate of the SPE mean, as high a gain as experimentally possible should be used and the value of the threshold cut must be chosen such that $k(f)/f$ is small.
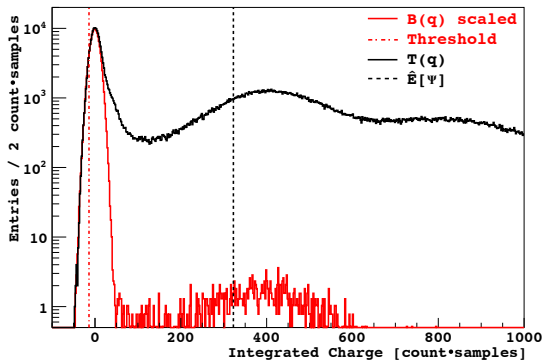
Figure 6: Same data as in Figure 4, with the blank data spectrum vertically scaled to match the laser data spectrum using the estimated occupancy. The dot-dashed vertical line indicates the position of the threshold cut, corresponding to $f = 0.1$, used to estimate the occupancy. The dashed vertical line indicates the value of the estimated single photoelectron mean.

It is difficult to calculate the systematic uncertainty in the estimation of the SPE variance and therefore, like the statistical uncertainty, it is also evaluated using simulations.

6.3. Choice of Threshold

As discussed above, the position of the threshold cut plays a key role in determining both the statistical and systematic uncertainty of the results. The position should be chosen to keep $k(f)$ (the fraction of the single photoelectron triggers falling below the cut) small in order to reduce the systematic bias, while still maintaining enough statistics f (fraction below the cut in the blank spectrum) to precisely estimate the occupancy. If experimentally possible, one should use Eq. (16) (depicted for our specific experimental setup in Figure 5) to choose the occupancy such that the required precision can be achieved with as low a threshold cut as possible, since the fractional bias $k(f)/f$ typically decreases as the cut value is decreased. If additional precision is desired, one can always increase the total number, N, of trigger samples acquired.

In order for the statistical uncertainty to remain below 3% for both the data acquired in our experimental setup and our Monte Carlo simulations, we have chosen our threshold cut to be $f = 0.1$ for occupancies in the range of $0.2 < \lambda$ [PE/trigger] < 8. For lower or higher occupancies we have chosen $f = 0.333$. Note that we have chosen to always place the cut such that $f < 0.5$, corresponding
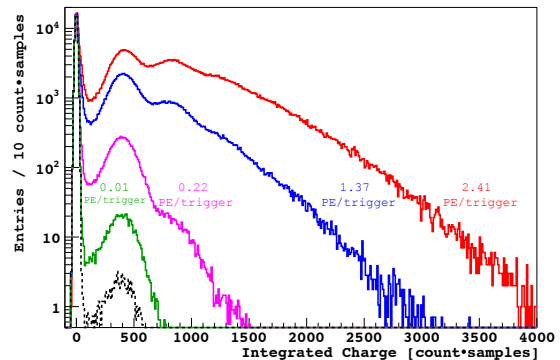

Figure 7: Integrated charge spectra for laser data sets acquired at a voltage difference of 1700 V with different light intensities ($\hat{\lambda}$ = 2.41, 1.37, 0.22 and 0.01 PE/trigger), along with the corresponding blank data set shown with a dashed line for comparison. The spectra are all scaled to have the same number of zero-pe triggers using the estimated occupancy.

to an integrated charge below zero (see for example the dot-dashed line in Figure 6). This implies that only very small single photoelectron signals (which when summed with the background noise lead to an overall negative charge) will fall below the threshold cut.

7. Experimental Results

It can be seen in Figure 6 that between 25 and 150 count·samples the excess of the laser spectrum above the blank spectrum differs significantly from a Gaussian tail, indicating the presence of a distinct population of under-amplified photoelectrons with low integrated charge. The mean of the single photoelectron distribution, as estimated by the method described in this paper, is shown by the dashed line in Figure 6. As one would expect, the presence of under-amplified photoelectrons with lower output charge pushes the estimated mean distinctly below the peak of the fully-amplified single photoelectron distribution. For the PMT and operating gain described above, the estimated mean of the entire single-photoelectron distribution, including under-amplified photoelectrons, is $\approx 80\%$ of the peak of the fully-amplified single-photoelectron distribution.

7.1. Dependence on Occupancy

In order to study the robustness of the method with respect to intensity of laser light used, several

9

Nominal Attenuation	Occupancy	SPE Mean	SPE Std. Dev.	SPE Rel. Std. Dev.
η	$\widehat{\lambda}$	$\widehat{E}[\psi]$	$\widehat{SD}[\psi]$	$\dfrac{\widehat{SD}[\psi]}{\widehat{E}[\psi]}$
	[PE/trigger]	[count·samples]	[count·samples]	
1E5	2.412 ± 0.015	321.6 ± 2.1	186.3 ± 1.7	0.579 ± 0.009
2E5	1.374 ± 0.010	317.1 ± 2.3	187.4 ± 1.9	0.591 ± 0.010
1E6	0.216 ± 0.006	314.4 ± 9.4	189.5 ± 8.0	0.603 ± 0.044
1E7	0.012 ± 0.003	388 ± 90	139 ± 30	0.36 ± 0.13

Table 1: Results for the estimated occupancy, single photoelectron mean and standard deviation for data acquired at a fixed PMT voltage difference (1700 V), with different optical filters to vary the intensity of laser light.

data sets were taken with the PMT supplied at a fixed voltage, but with optical fibers providing different levels of attenuation of the laser light. The observed occupancy did not exactly scale with the nominal filter attenuation used because different numbers and combinations of filters were used to obtain the different light intensities and reflections can occur between the filters. Figure 7 shows the laser spectra we obtained, where the distributions have been normalized to have the same number of zero-pe triggers, based on the occupancy calculated as described in Section 5. The resulting estimates for the single photoelectron mean and standard deviation, $\widehat{SD}[\psi] \equiv \sqrt{\widehat{V}[\psi]}$, are shown in Table 1. It can be seen that this method produces consistent results for the SPE mean and variance, with statistical uncertainties below 3% and 4% respectively, over a range of occupancies that span from 0.2 to 2.4 PE/trigger. At the lowest occupancy measured of $\lambda = 0.01$ PE/trigger the values obtained are still consistent with the other measurements, though the statistical uncertainties are too large for most applications. Better precision can be obtained simply by increasing the number of trigger samples acquired. While our experimental data only extend up to an occupancy of 2.41 PE/trigger, Eq. (16) indicates that for the parameters of this experimental setup, and a suitable choice of threshold as described in Section 6.3, the method has a statistical uncertainty of less than 3% on the SPE mean for occupancies spanning nearly two orders of magnitude from 0.1 to 9.5 PE/trigger. This method is therefore especially useful for large detectors that contain an array of photomultiplier tubes, where a uniform illumination of the PMTs may not be possible.
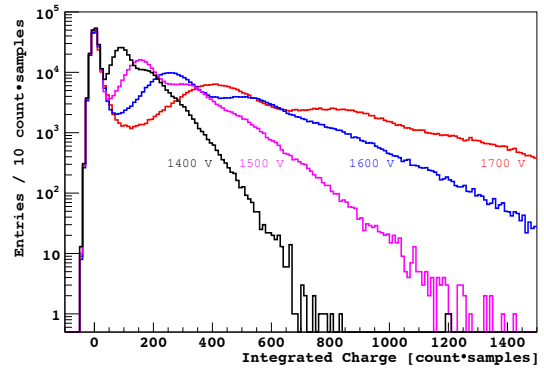

Figure 8: Integrated charge spectra for laser data sets acquired at a fixed laser intensity ($\widehat{\lambda} = 1.37$ photoelectrons/trigger) with varying PMT voltage differences (1400 V, 1500 V, 1600 V, 1700 V).

7.2. Dependence on Gain

As described in Section 6.2, the systematic uncertainty on the estimated SPE mean is related to the fraction of single photoelectron triggers falling below the threshold cut. One way the uncertainty can be reduced is by increasing the voltage applied to the PMT, thereby increasing the gain. However, in some experimental setups it is often not possible to run PMTs at high gain values due to dynamic range limitations or the emission of light from internal PMT structures [16]. To study the performance of the method at lower gain, data sets were acquired at a constant laser intensity but varying voltage differences applied to the PMT (shown in Figure 8).

Since the method described above uses a simple threshold cut to estimate the occupancy, the overlapping of the noise and under-amplified photoelectrons makes it difficult to accurately estimate the occupancy and hence the single photoelectron mean and variance. The estimated occupancy is
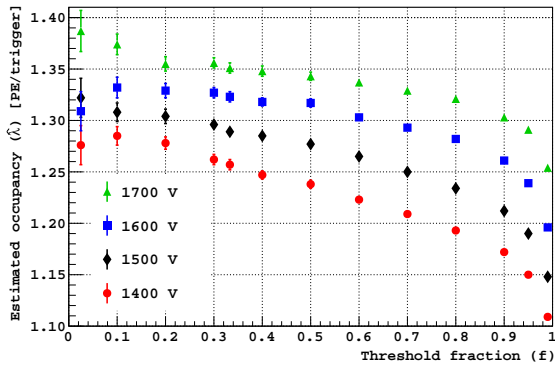
10

Figure 9: Estimated occupancy for laser data sets acquired at a fixed light intensity with varying PMT voltage differences (1400 V, 1500 V, 1600 V, 1700 V) as a function of the fraction of single photoelectron triggers falling below the threshold cut (f).
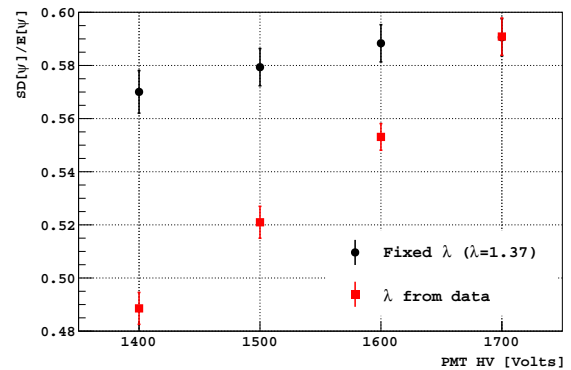

Figure 10: Estimated single photoelectron relative standard deviation for data acquired at a fixed light intensity with varying PMT voltage differences. Circles: For all voltages the occupancy was set to the occupancy estimated at the highest gain and $f = 0.1$ (1.37 PE/trigger). Squares: The occupancy was estimated independently at each of the corresponding voltages and $f = 0.1$.

shown in Figure 9 as a function of the chosen threshold fraction f, for different PMT voltages. It can be seen that choosing a lower threshold leads to an increase in the estimated occupancy. This is because as one lowers the threshold the fraction of underamplified photoelectrons falling below the threshold reduces and the systematic bias in the estimate of the occupancy is lower (see Section 6.2). Similarly, running at higher PMT gains also decreases the fraction of underamplified photoelectrons falling below the threshold. The fractional variation in the estimated occupancy leads to roughly the same size fractional variation in the estimated SPE mean, though in the opposite direction.

It should be noticed that even at a relatively low thresholds ($f \leq 0.1$), the estimated occupancy decreases slightly as one lowers the PMT gain. While there may be some small loss of photomultiplier efficiency at lower voltages due to inefficient focussing in the dynode structure, as we will see from the simulation studies in Section 8, the decrease in estimated occupancy (and correspondingly increase in estimated SPE mean) is consistent with the expected systematic bias described in Section 6. More sophisticated algorithms that rely on other parameters to estimate the occupancy will likely be less biased at low gains.

Since the systematic bias increases as one lowers the gain, rather than trying to estimate the occupancy at each gain setting, one can fix the occupancy to the estimated value obtained at the highest gain, where the bias is least. We can compare

the previous results with those using a fixed occupancy by comparing the estimated SPE relative standard deviation, $\widehat{SD}[\psi]/\widehat{E}[\psi]$, which should remain roughly constant at all gain values (provided the PMT collection efficiency remains constant). Figure 10 shows that when fixing the occupancy to the value obtained at 1700 V the relative standard deviation is constant within 3%, as compared to a 17% variation when one uses the estimated occupancy obtained at each of the corresponding PMT voltages. Thus, for applications in which the photomultiplier is required to be calibrated at low gain, it is recommended to estimate the occupancy by temporarily running the PMT at a higher gain, while keeping the laser intensity constant. This value of the occupancy, estimated at higher gain, can then be used to calculate the single photoelectron mean and variance at the desired lower operating gain. If it is not possible to temporarily increase the PMT gain, the systematic bias in the estimated single photoelectron moments can be evaluated using simulations, as discussed in the following section.

8. Simulation

In order to verify that the single photoelectron calibration method described in this paper works accurately not only for the specific photomultiplier and conditions studied in the experimental setup, but also for different single photoelectron spectra, light intensities, and PMT gain, a Monte
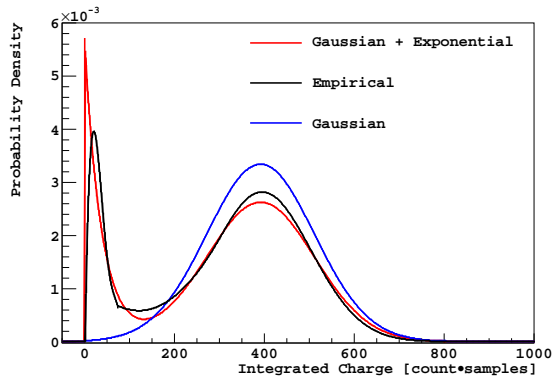
Figure 11: Different spectral shapes used as single photoelectron distributions in the Monte Carlo simulations. The empirical distribution is a combination of a Gaussian distribution and an under-amplified component whose shape was obtained from the difference of the experimentally measured laser and blank spectra.

Carlo generator was written to simulate laser-induced PMT pulses and overlay them on background waveforms acquired during blank data sets. The simulated events were then processed in the same manner as the experimental data and the estimated single photoelectron moments were compared to the simulated inputs as a function of the gain, occupancy, and shape of the single photoelectron spectrum. To understand the systematic bias of the method we compared the mean value of the estimated moments, averaged over a large number of trials, to the simulated input; the standard deviation of the estimated moments was taken as the statistical uncertainty of the method. The simulation of each event in a given configuration begins by drawing a random number of photoelectrons from a Poisson distribution with a fixed mean corresponding to the desired occupancy. The integrated charge corresponding to each photoelectron was then independently drawn from a SPE spectrum. Since the true shape of the SPE charge spectrum is not known, three different approximations of the SPE spectra were studied. The first spectrum was approximated from the experimental data, combining a Gaussian peak (representing the fully amplified photoelectron distribution) with an under-amplified distribution that was obtained by subtracting the scaled blank spectrum from the laser spectrum acquired at the highest gain and occupancy. This empirically derived SPE spectrum, shown in Figure 11, displays a prominent peak at low charge values,

very similar to the shapes obtained in other experimental setups for a variety of different photomultiplier tubes [4, 8, 10]. It should be noted that though this empirically derived shape serves as a good approximation of the true SPE spectrum for the purposes of these simulation studies, it is not entirely accurate because the data from which it was derived included contributions from electronics noise present in each trigger as well as multiple photoelectrons. We considered two other shapes as potential extreme cases: a simple Gaussian truncated at zero, representative of a single photoelectron distribution without any contribution from under-amplified photoelectrons, and a Gaussian with an under-amplified distribution that rises exponentially at low charge values [9]. For the latter two distributions, shown in Figure 11, the shape of the spectra were tuned to try and match our experimental data as well as possible. In order to simulate different gains, the spectra were linearly scaled such that the peak of the Gaussian matched the experimental data at each PMT high voltage value. For each simulated photoelectron a waveform is generated based on measurements of the single photoelectron pulse shape. The integral of the pulse is scaled to equal the charge assigned to the photoelectron and the peak time is set to match the arrival time of the PMT signal in the experimental setup. The pulses corresponding to all the photoelectrons in a given event are then summed together and overlaid on top of a waveform acquired during a blank data set taken in the same configuration, accounting for the discreteness of the ADC samples in time and amplitude. The use of the experimentally obtained waveforms from the blank data set allows us to accurately include all of the relevant effects such as noise, stray photoelectrons and dark current into the simulation. Each simulated waveform is processed identically to the experimental data in order to obtain the estimates of the SPE mean and variance.

8.1. Dependence on Gain

Using the results of the simulation, we studied the effects of the systematic bias observed in the experimental data (Section 7.2) for the three different single photoelectron spectra as a function of the PMT gain. At lower gains the bias is expected to increase due to the increasing fraction of single photoelectron triggers falling below
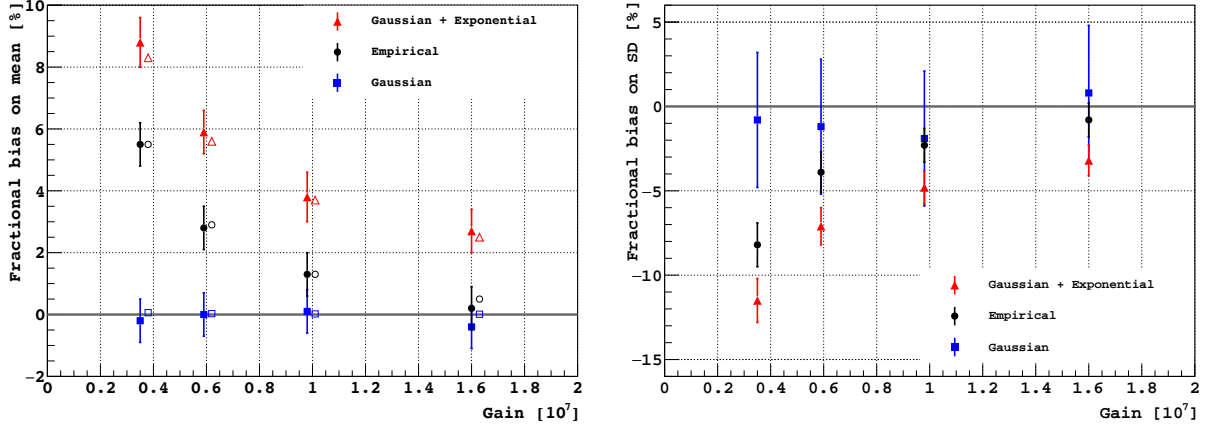
Figure 12: Simulation results for a fixed occupancy (1.37 PE/trigger), with varying gain. Left: Fractional bias in the estimated single photoelectron mean $\left(\frac{E\left[\widehat{E}[\psi]\right] - E_{sim}[\psi]}{E_{sim}[\psi]} \right)$. Right: Fractional bias in the estimated standard deviation $\left(\frac{E\left[\widehat{SD}[\psi]\right] - SD_{sim}[\psi]}{SD_{sim}[\psi]} \right)$. The filled markers indicate the fractional bias of the model independent method for the different simulated single photoelectron distributions, while the error bars depict the fractional statistical uncertainty of the method. The open markers on the left (horizontally displaced for clarity) indicate the analytic calculation of the fractional bias in the mean for each case (see Eq. (18)).
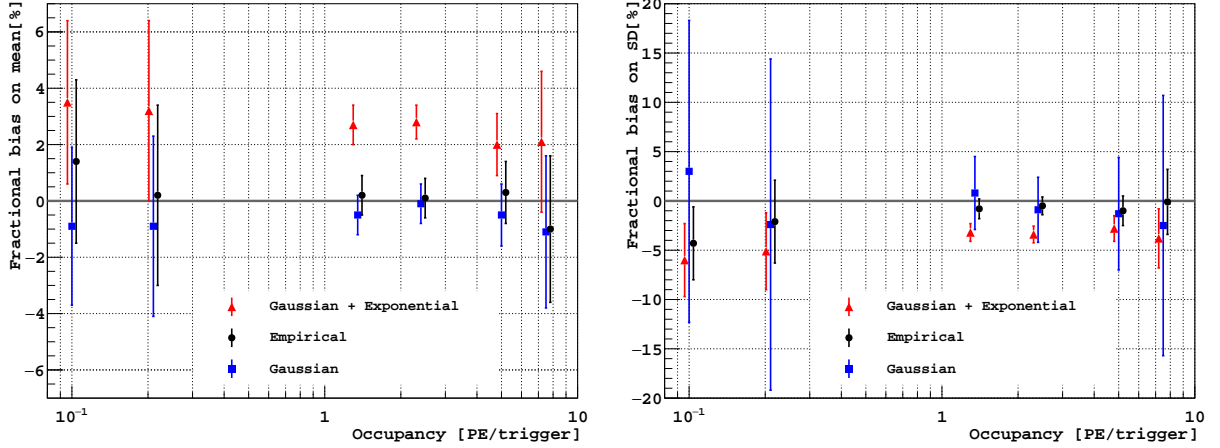

Figure 13: Simulation results for a fixed gain (1.6×10^7), with varying occupancy. Left: Fractional bias in the estimated single photoelectron mean $\left(\frac{E\left[\widehat{E}[\psi]\right] - E_{sim}[\psi]}{E_{sim}[\psi]} \right)$. Right: Fractional bias in the estimated standard deviation $\left(\frac{E\left[\widehat{SD}[\psi]\right] - SD_{sim}[\psi]}{SD_{sim}[\psi]} \right)$. The markers indicate the fractional bias of the model independent method for the different simulated single photoelectron distributions (horizontally displaced for clarity), while the error bars depict the fractional statistical uncertainty of the method.

the threshold cut. In Figure 12 we report the results of the simulation for single photoelectron gain settings corresponding to the PMT HV supply values used in the experimental setup, and an occupancy of 1.37 PE/trigger. As expected, the systematic bias is larger at lower gains and for simulated SPE spectra with a larger under-amplified component. The consistency between

the simulation results (closed circles) and the estimated systematic uncertainty in Eq. (18) (open circles), indicates that the analytical model derived in Appendix B is accurate. For a truly Gaussian SPE spectrum the estimates of the mean and variance of the SPE response are unbiased at all gains, while for the empirical SPE spectrum obtained from the experimental measurements of the

13

R11410, the bias on the mean (standard deviation) ranges from 0% to +5% (-1% to -8%), depending on the gain. These values closely match the variations in the experimental data presented in Section 7.2, suggesting that the simulation accurately represents the experimental data. It should be noted that in the worst case considered, with an exponentially increasing under-amplified spectrum and low PMT gain, the systematic bias in the single photoelectron mean and standard deviation of +8% and -12% respectively is significantly lower than the bias one would obtain by ignoring the under-amplified electrons and only fitting the Gaussian component (+20% and -50% respectively).

8.2. Dependence on Occupancy

In order to test the sensitivity of the method to the intensity of the laser light, we simulated datasets at various occupancies for all three different single photoelectron spectra at a gain equivalent to the experimental data taken at 1700 V. The results are shown in Figure 13, where it can be seen that the estimates are consistent with the simulated single photoelectron moments (after accounting for the small systematic bias discussed above). This confirms the validity of the method for a wide range of PMT illumination. The larger fractional statistical uncertainty of the estimated SPE standard deviation obtained with the Gaussian SPE spectrum, as compared to the other spectra, is due to the larger ratio of the SPE mean to variance (see Eq. (17)).

8.3. Comparison with fit methods

Finally, we compare the model independent method presented in this paper with more conventional fit methods. We have chosen two commonly used fitting methods which approximate the SPE response as either a simple Gaussian distribution or a Gaussian + exponential [9]. For both methods, the response to p photoelectrons is assumed to be the $p-$times repeated convolution of the SPE response, additionally convolved with a single Gaussian distribution representing the noise. Aside from specifying the shape of both the single photoelectron and noise response, these are the same underlying assumptions as the model independent method. We apply the fitting techniques to the simulated spectra that were generated with the empirically determined SPE spectrum. Since the repeated convolution of a Gaussian + exponential is difficult to calculate exactly for more than 2 photoelectrons, we have restricted the comparison to a simulated data set with relatively low occupancy (0.22 PE/trigger), to avoid biasing the fit results. Figure 14 shows the comparison of the bias in the estimated single photoelectron mean and standard deviation for the model independent method and the two fit methods. It can be seen that the model independent method provides a more accurate estimate than either of the fit methods at all gain values. The fit methods have comparatively smaller statistical uncertainties, though, as shown earlier, the statistical uncertainty of the model independent method can be reduced by either operating at higher occupancy or acquiring more statistics.

9. Conclusions

In this paper we have presented a simple new method to calibrate the single photoelectron response of photomultiplier tubes, taking into account the important contributions of under-amplified photoelectrons. Unlike conventional fitting methods, the proposed procedure determines the single photoelectron mean and variance statistically, without making any assumption about the underlying shape of the single photoelectron spectrum. It can therefore be used to calibrate PMTs with different dynode structures, regardless of the fraction of under-amplified photoelectrons or the features of the single photoelectron charge spectrum. The method is shown to work well over a wide range (nearly two orders of magnitude) of light intensities and is therefore also suitable for the calibration of arrays of photomultipliers in large detectors, where uniform illumination is not possible. Following the description of the method, we have outlined the procedure to estimate the required parameters and their uncertainties, and applied the method to experimental data acquired with a Hamamatsu R11410 photomultiplier. Additionally we have used a Monte Carlo simulation with experimentally measured noise levels to study the results of the method as a function of the single photoelectron spectrum, photomultiplier gain, and light intensity. The method is found to estimate the single photoelectron mean and variance to better than 5% for all single photoelectron spectra considered, at PMT gain values above 1×10^7. At lower gains,
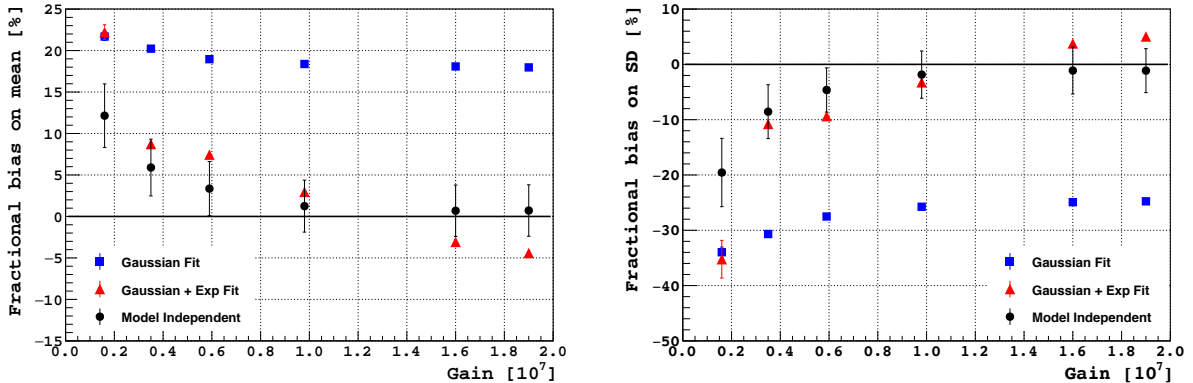
Figure 14: Comparison of the estimated single photoelectron mean and standard deviation to more conventional fitting methods for a fixed occupancy (0.22 PE/trigger), with varying gain. The markers indicate the fractional bias while the error bars depict the fractional statistical uncertainty of the method.

a small systematic bias is present due to the overlap of the under-amplified spectra with the noise; this bias can be reduced by temporarily raising the gain to accurately evaluate the occupancy or by the use of more sophisticated algorithms to distinguish between the signals and the background noise of the specific setup. Simulations using the SPE spectrum derived from our measurements of the R11410 PMT show that the method described here is more accurate than conventional fitting algorithms at all gain values. We note that our SPE spectrum is similar in shape to those obtained in other experimental setups with other PMT models [4, 8, 10], suggesting that our method has broad application.

10. Acknowledgements

Appendix A.

From Eq. (7), the statistical uncertainty on the single photoelectron mean can be written as

$$V\left[\widehat{E}\left[\psi\right]\right] \approx \frac{V\left[\widehat{E}\left[T\right]\right] + V\left[\widehat{E}\left[B\right]\right] + E^2\left[\psi\right] \cdot V\left[\widehat{\lambda}\right]}{E^2\left[\widehat{\lambda}\right]}$$
(A.1)

where $\widehat{E}\left[X\right]$ denotes the estimated mean, *i.e.* the estimate of the mean of the distribution X from the finite data sample taken and for convenience we have defined $\widehat{\lambda} \equiv \widehat{E}\left[L\right]$. We have ignored the smaller correlation terms.

Since the estimated mean of the total charge distribution, $\widehat{E}\left[T\right]$, is evaluated by calculating the arithmetic mean of the sampled distribution, the variance of the estimate is simply

$$V\left[\widehat{E}\left[T\right]\right] = \frac{V\left[T\right]}{N_L}$$
(A.2)

where N_L is the number of sample triggers in the laser data. Using Eq. (9), one can write

$$V\left[\widehat{E}\left[T\right]\right] = \frac{E\left[L\right] \cdot \left(E^2\left[\psi\right] + V\left[\psi\right]\right) + V\left[B\right]}{N_L}$$
(A.3)

Similarly to $\widehat{E}\left[T\right]$ and considering that N_B is the number of sample triggers in the blank data, the variance of the estimate $\widehat{E}\left[B\right]$ is

$$V\left[\widehat{E}\left[B\right]\right] = \frac{V\left[B\right]}{N_B}$$
(A.4)

15

The mean and variance of the estimate of the occupancy, $\widehat{\lambda} \equiv -\ln{(A_T/fN)}$, (excluding any bias from non-zero-pe triggers leaking below the amplitude cut) can be evaluated by first calculating the mean and variance of A_T, which is the number of zero-pe triggers that fall below the threshold. If the position of the threshold cut was fixed, then A_T would follow a simple Binomial distribution. However, the position of the threshold cut is chosen based on the randomly sampled background distribution and is therefore a random variable itself. Thus the statistical uncertainty on A_T depends on the fluctuations of two random processes:

1. Fluctuations in defining the position of the threshold cut based on the background events.

2. Fluctuations in the number of laser events falling below the threshold.

The fraction of the background distribution $B(q)$ that falls below a given charge value q is simply the value of the cumulative background distribution, defined as $F_B(q)$. If the charge q is itself sampled from the background distribution, then $F_B(q)$ is also a random variable that follows a uniform distribution. The position of the threshold cut q_t is chosen to be the charge value of the $j = f \cdot (N_B + 1)^{th}$ *ordered* sample of the N_B acquired background samples. Since the cumulative distribution is strictly increasing, it preserves order statistics and the fraction of the background distribution that falls below q_t also corresponds to the value of the jth ordered sample of the uniform distribution $F_B(q)$. The jth order statistic of a uniform distribution is a beta random variable, and therefore $\phi_t \equiv F_B(q_t)$ follows a beta distribution $\text{Beta}(\alpha, \beta)$ with $\alpha \equiv j$, and $\beta \equiv N_B - j + 1 \equiv (1 - f) \cdot (N_B + 1)$.

$$\text{Beta}(\phi_t|j, N_B - j + 1) = \frac{N_B!}{(j-1)!(N_B - j)!}\phi_t^{j-1}\phi_t^{N_B - j} \tag{A.5}$$

We can therefore analytically calculate the mean

and variance of the distribution of ϕ_t

$$E[\phi_t] = \frac{\alpha}{\alpha + \beta} = \frac{j}{N_B + 1} = f \tag{A.6}$$

$$V[\phi_t] = \frac{\alpha\beta}{(\alpha + \beta)^2(\alpha + \beta + 1)}$$
$$= \frac{f(1 - f)}{N_B + 2} \tag{A.7}$$

As expected, the distribution of ϕ_t is unbiased with the mean equal to f and its variance goes to 0 for large N_B.

Now, in the laser data set, we define the number of triggers that fall below q_t to be A_T. A_T does not follow a simple Binomial distribution, but instead follows a Binomial distribution where for each set of N_B blank samples, the threshold q_t varies according to the Beta distribution given above, and hence the probability of a zero-pe laser sample falling below q_t varies.

$$A_T \sim \text{Binom}(N_L, L(0)\phi_t) \tag{A.8}$$
$$\phi_t \sim \text{Beta}(\alpha, \beta) \tag{A.9}$$

Note that for $L(0) = 1$, the distribution of A_T would reduce to a standard beta-binomial distribution. One can compute the first two central moments using the following relations for mixture distributions:

$$E[A_T] = \sum_{m=0}^{\infty} m \int_0^1 \text{Binom}(m|N_L, L(0)f) \cdot \text{Beta}(\phi_t|\alpha, \beta)d\phi_t$$
$$= N_L L(0) f \tag{A.10}$$

$$V[A_T] = \sum_{m=0}^{\infty} m^2 \int_0^1 \text{Binom}(m|N_L, L(0)f) \cdot \text{Beta}(\phi_t|\alpha, \beta)d\phi_t$$
$$- E^2[A_T]$$
$$= N_L L(0) f \left[(1 - L(0)f) + \left(\frac{N_L - 1}{N_B + 2}\right)L(0)(1 - f)\right]$$
$$\approx N_L L(0) f[(1 - L(0)f) + L(0)(1 - f)] \tag{A.11}$$

where in the last step we have used $N_L = N_B \equiv N \gg 1$ which we will assume from now on.

We can then write the mean and variance of the occupancy $\widehat{\lambda} \equiv -\ln{(A_T/fN)}$ as

$$E\left[\widehat{\lambda}\right] \approx -\ln{(L(0))} = \lambda \tag{A.12}$$

$$V\left[\widehat{\lambda}\right] \approx \frac{(L(0)^{-1} + 1 - 2f)}{fN} \tag{A.13}$$

$$= \frac{(e^\lambda + 1 - 2f)}{fN} \tag{A.14}$$

Combining the individual statistical uncertainties from Eqs. (A.3), (A.4), (A.12), and (A.13) into Eq. (A.1), we get

$$V\left[\widehat{E}\left[\psi\right]\right] \approx \frac{\lambda(E^2\left[\psi\right] + V\left[\psi\right]) + 2V\left[B\right]}{N\lambda^2} + \frac{E^2\left[\psi\right]\left(e^\lambda + 1 - 2f\right)}{fN\lambda^2} \quad \text{(A.15)}$$

This can also be expressed in terms of the first two moments from the blank and laser distributions ($E\left[T\right]$, $E\left[B\right]$, $V\left[T\right]$, $V\left[B\right]$)

$$V\left[\widehat{E}\left[\psi\right]\right] \approx \frac{V\left[T\right] + V\left[B\right]}{N\lambda^2} + \frac{(E\left[T\right] - E\left[B\right])^2\left(e^\lambda + 1 - 2f\right)}{fN\lambda^4}$$

$$\text{(A.16)}$$

Appendix B.

The presence of laser-induced photoelectron signals below the threshold cut can bias the estimated occupancy and consequently the estimated single photoelectron mean. The number of these non-zero-pe triggers, l, leaking below the threshold cut can be reasonably expected to be proportional to the number of events that produce exactly one photoelectron, since the probability of two or more photoelectrons producing a combined signal that falls below the threshold cut should be negligible. One can then write, l, the mean number of leakage events as

$$l = k(f) \cdot N \cdot L(1)$$
$$= k(f) \cdot N \cdot \lambda \cdot L(0) \quad \text{(B.1)}$$

where $k(f)$ is the fraction of triggers with exactly one laser-induced photoelectron, whose total charge falls below the threshold cut.

Triggers with laser-induced single photoelectrons that fall below the threshold cut lead to an overestimate of A_T, the number of zero-pe triggers below the cut

$$E\left[A_T\right] = NL(0)f + l$$
$$= NL(0)f\left(1 + \frac{k(f)}{f}\lambda\right)$$

This translates into biased estimates of the occupancy $\widehat{\lambda}$ and the single photoelectron mean $\widehat{E}\left[\psi\right]$

$$E\left[\widehat{\lambda}\right] = E\left[-\ln\left(A_T/fN\right)\right]$$
$$\approx \lambda - \ln\left(1 + \frac{k(f)}{f} \cdot \lambda\right)$$
$$\approx \lambda \cdot \left(1 - \frac{k(f)}{f}\right) \quad \text{(B.2)}$$

$$E\left[\widehat{E}\left[\psi\right]\right] \approx E\left[\psi\right] \cdot \left(1 + \frac{k(f)}{f}\right) \quad \text{(B.3)}$$

where we have assumed that $k(f)/f \ll 1$.

References

References

[1] E. Bellamy, G. Bellettini, J. Budagov, F. Cervelli, I. Chirikov-Zorin, M. Incagli, D. Lucchesi, C. Pagliarone, S. Tokar, F. Zetti, Absolute calibration and monitoring of a spectrometric channel using a photomultiplier, Nuclear Instruments and Methods in Physics Research Section A: Accelerators, Spectrometers, Detectors and Associated Equipment 339 (1994) 468 – 476.

[2] J. Prescott, A statistical model for photomultiplier single-electron statistics, Nuclear Instruments and Methods 39 (1966) 173 – 179.

[3] F. J. Lombard, F. Martin, Statistics of electron multiplication, Review of Scientific Instruments 32 (1961) 200–201.

[4] A. G. Wright, Method for the determination of photomultiplier collection efficiency, F, Appl. Opt. 49 (2010) 2059–2065.

[5] F. Kaether, C. Langbrandtner, Transit time and charge correlations of single photoelectron events in R7081 photomultiplier tubes, Journal of Instrumentation 7 (2012) P09002.

[6] S.-O. Flyckt, C. Marmonier, Photomultiplier tubes: principles and applications, Photonis, Brive, France, 2002.

[7] D. Carter, Photomultiplier Handbook: Theory, Design, Application, Lancaster, Pennsylvannia: Burle Industries, Inc., 1980.

[8] J. de Haas, P. Dorenbos, Methods for accurate measurement of the response of photomultiplier tubes and intensity of light pulses, Nuclear Science, IEEE Transactions on 58 (2011) 1290–1296.

[9] R. Dossi, A. Ianni, G. Ranucci, O. Smirnov, Methods for precise photoelectron counting with photomultipliers, Nuclear Instruments and Methods in Physics Research Section A: Accelerators, Spectrometers, Detectors and Associated Equipment 451 (2000) 623 – 637.

[10] I. Chirikov-Zorin, I. Fedorko, A. Menzione, M. Pikna, I. Sykora, S. Tokar, Method for precise analysis of the metal package photomultiplier single photoelectron spectra, Nuclear Instruments and Methods in Physics Research Section A: Accelerators, Spectrometers, Detectors and Associated Equipment 456 (2001) 310 – 324.

[11] B. E. Saleh, M. C. Teich, Fundamentals of Photonics, volume 22, John Wiley & Sons, Inc., 1991.

[12] Y. Hu, X. Peng, T. Li, H. Guo, On the Poisson approximation to photon distribution for faint lasers, Physics Letters A 367 (2007) 173 – 176.

[13] M. C. Teich, B. E. A. Saleh, Effects of random deletion and additive noise on bunched and antibunched photon-counting statistics, Opt. Lett. 7 (1982) 365–367.

[14] Hamamatsu photonics, Accessed: 6th July 2016. URL: https://www.hamamatsu.com/resources/pdf/etd/High_energy_PMT_TPMO0007E.pdf.

[15] CAEN V1720 Digitizer, Accessed 11th September 2015. URL: http://www.caen.it/csite/CaenProd.jsp?idmod=570&parent=11.

[16] D. Akimov, A. Bolozdynya, Y. Efremenko, V. Kaplin, A. Khromov, Y. Melikyan, V. Sosnovtsev, Observation of light emission from Hamamatsu R11410-20 photomultiplier tubes, Nuclear Instruments and Methods in Physics Research Section A: Accelerators, Spectrometers, Detectors and Associated Equipment 794 (2015) 1 – 2.